frontiers | Frontiers in Physics

TYPE Original Research
PUBLISHED 11 October 2022
DOI 10.3389/fphy.2022.1037821

OPEN ACCESS

EDITED BY
Minbiao Ji,
Fudan University, China

REVIEWED BY
Wei Zheng,
Shenzhen Institutes of Advanced Technology (CAS), China
Jiong Ma,
Fudan University, China

*CORRESPONDENCE
Ke Si,
kesi@zju.edu.cn

†These authors have contributed equally to this work

SPECIALTY SECTION
This article was submitted to Optics and Photonics,
a section of the journal
Frontiers in Physics

RECEIVED 06 September 2022
ACCEPTED 26 September 2022
PUBLISHED 11 October 2022

CITATION
Xu X, Zheng Y, Xiao X, Wang Z, Lv J, Wang Y, Zhang J, Duan S and Si K (2022), FOCMS: An ultrafast optical clearing method with quantified analysis. *Front. Phys.* 10:1037821. doi: 10.3389/fphy.2022.1037821

FOCMS: An ultrafast optical clearing method with quantified analysis

Xiaobin Xu[1,2,3†], Yameng Zheng[2,3†], Xiao Xiao[2,4†], Zizheng Wang[4], Jie Lv[5], Yongjie Wang[6], Jianmin Zhang[6], Shumin Duan[2,3] and Ke Si[1,2,3,4,7*]

[1]Department of Psychiatry of the First Affiliated Hospital, Zhejiang University School of Medicine, Hangzhou, China, [2]MOE Frontier Science Center for Brain Science & Brain-Machine Integration, NHC and CAMS Key Laboratory of Medical Neurobiology, School of Brain Science and Brain Medicine, Zhejiang University, Hangzhou, China, [3]Liangzhu Laboratory, Zhejiang University Medical Center, Hangzhou, China, [4]College of Optical Science and Engineering, Zhejiang University, Hangzhou, China, [5]School of Software Technology, Zhejiang University, Ningbo, China, [6]Department of Neurosurgery of the Second Affiliated Hospital, Zhejiang University School of Medicine, Hangzhou, China, [7]Intelligent Optics and Photonics Research Center, Jiaxing Research Institute, Zhejiang University, Jiaxing, China

Optical clearing technology offers a prospective solution to improve the imaging depth and quality of optical microscopy, but there is still a lack of quantitative standards to accurately evaluate transparency effects so the composition and concentration of most reagents are not optimal. Here, we propose a transparency quantitative analysis method (TQAM) based on the tissue area recognition technique to achieve the high-throughput reagent concentration gradient screening. After optimizations of reagent composition, concentration, operation time and other parameters of the optical clearing, we develop a new ultrafast optical clearing method with quantified analysis (FOCMS) with excellent transparency effect, simple operation, improved imaging depth and quality, minor morphological change and outstanding fluorescence retention. Applied the FOCMS to an application of human brain tissue, significant differences are observed between glioma and normal human brain tissue, while these differences are difficult to be found without the assistance of FOCMS. Therefore, FOCMS shows great application potential in clinical diagnosis and treatment, pathological analysis and so on.

KEYWORDS

ultrafast optical clearing, transparency quantitative analysis, human brain, glioma, deep tissue imaging

Introduction

High resolution optical imaging of deep biological tissue shows great significance in the fields of tissue structure and medical diagnosis [1]. However, the strong scattering and high turbidity in biological tissue greatly hinder the penetration capability and imaging quality of the optical imaging system. Various optical imaging systems such as laser scanning confocal imaging (LSCM) [2], multiphoton imaging [3], stimulated Raman

scattering imaging [4], and photoacoustic imaging [5] have been developed to improve the penetration depth, but they are usually suffered from low imaging speed and high cost [6]. Moreover, these optical imaging systems are not enough to satisfy the requirements for biological studies such as whole brain or organ imaging [7, 8]. Optical clearing is a promising method utilizing refractive index matching and tissue decolorization, which greatly reduces the scattering of biological tissue and significantly improves the penetration depth and resolution [9–12].

There are three major clearing methods including organic solvent-based tissue clearing, aqueous-based tissue clearing, and hydrogel embedding tissue clearing. The DISCO [13, 14] technology based on organic solvents achieves the transparency of large-volume biological tissues, and transparency of intact human organs has been obtained with the development of the SHANEL method [7]. However, this organic solvent-based tissue clearing method causes tissue deformation, especially for large tissues and requires a complex operation. The aqueous-based tissue clearing technologies such as SeeDB [15], Scale [16], and CUBIC [17], have successfully achieved versatile whole-organ staining and imaging [17, 18]. They have the advantages of simple and safe operation, and good fluorescence preservation, but suffer from long clearing time and poor clearing efficiency. The advancement of the hydrogel embedding tissue clearing method well improves the optical clearing efficiency and maintains the integrity of the tissue morphology. However, high concentrations of detergents and harsh treatments may result in the loss of native biomolecules and damage to tissue architecture [12, 19, 20]. Optical clearing method is often combined with light sheet microscopy to achieve rapid three-dimensional imaging of organs and even the whole body [21]. The previous clearing methods are designed to be transparent to large biological tissues, however, they have defects of either severe fluorescence quenching, long clearing time, morphology distortion or complicated operations, which seriously limit the applications in combing with commonly used optical imaging systems such as LSCM and two-photon microscopy. We recently proposed a fast optical clearing method (FOCM) with simple protocols and common reagents, achieving efficient transparency, easy operation and less fluorescence toxicity [22]. Current optical clearing approaches use human eyes to evaluate the transparency effect in most scenarios, however, there is still a lack of accurate quantitative evaluation standards for the transparency effect. Thus, the composition and concentration of reagents are not optimal.

To solve this issue, quantitative measurements of optical clearing have recently been developed using spectrophotometer [8] and microplate reader [23], but these are not widely used due to the high cost of measurement devices. Here, we propose the TQAM based on the brain slice area recognition technique, which achieves high-throughput gradient screening of reagent concentrations. This concentration gradient screening benefits the optimization of the reagent composition, concentration, operation time and other parameters of the optical clearing, and the mutual comparison of various optical clearing reagents. Through the concentration gradient screening, we propose a novel ultrafast optical clearing method, FOCMS, only consisting of DMSO and urea. This paper focuses on optimizing the optical clearing performances on time, imaging depth and quality, transparency effect and fluorescence retention, and expands the application scenarios of FOCMS optical clearing technology. Taking human glioma as an example, we find that there are distinct differences between glioma and normal human brain tissue, however, these differences are difficult to be observed if the tissue is not cleared by FOCMS. Therefore, the FOCMS optical clearing technology is expected to greatly promote its application in clinical diagnosis and treatment, pathological analysis and other fields with the combination of optical imaging systems.

Material and method

Experimental procedure and method

For traditional immunofluorescence imaging, the mice were first subjected to operations including anesthesia, perfusion, brain removal, and sectioning, followed by immunofluorescence staining of brain slices, and finally mounting and imaging, shown in Figure 1A. To improve the quality of immunofluorescence imaging, FOCMS is a method that contains optical clearing after immunofluorescence staining, and this optical clearing process only takes 5 min to complete which is less than the imaging preparation time.

Immunofluorescence staining. After decolorization, brain slices were incubated with primary antibodies in PBST (0.01 M PBS with 0.1% Triton X-100) at 37°C for 48–96 h with shaking, followed by washing at 37°C for 1 h in PBST three times. Then incubated with secondary antibodies under the same conditions.

Optical Clearing Method. PBST should be sopped up by KimWipes after washing and labeling samples. The sample only needs to incubate for 3–10 min using 600 μl FOCMS reagent at room temperature in dishes. After FOCMS clearing Figure 1B, the sample should be mounted (Figure 1C) immediately to isolate air.

Laser Scanning Confocal Microscopy (LSCM). An inverted confocal microscopy FV1000 (Olympus) was used to perform fluorescence imaging of the brain section. A He-Ne laser (543.5 nm) and laser diode (473 and 635 nm) were used as the light source. To acquire the fluorescent images, we used different objective lenses including a ×20 air objective lens (Olympus, UPLSAPO ×20, N.A.0.75, WD 0.6 mm), ×40 air objective lens (Olympus, UPLSAPO ×40, N.A.0.95, WD 0.18 mm) and ×60 oil objective lens (Olympus,

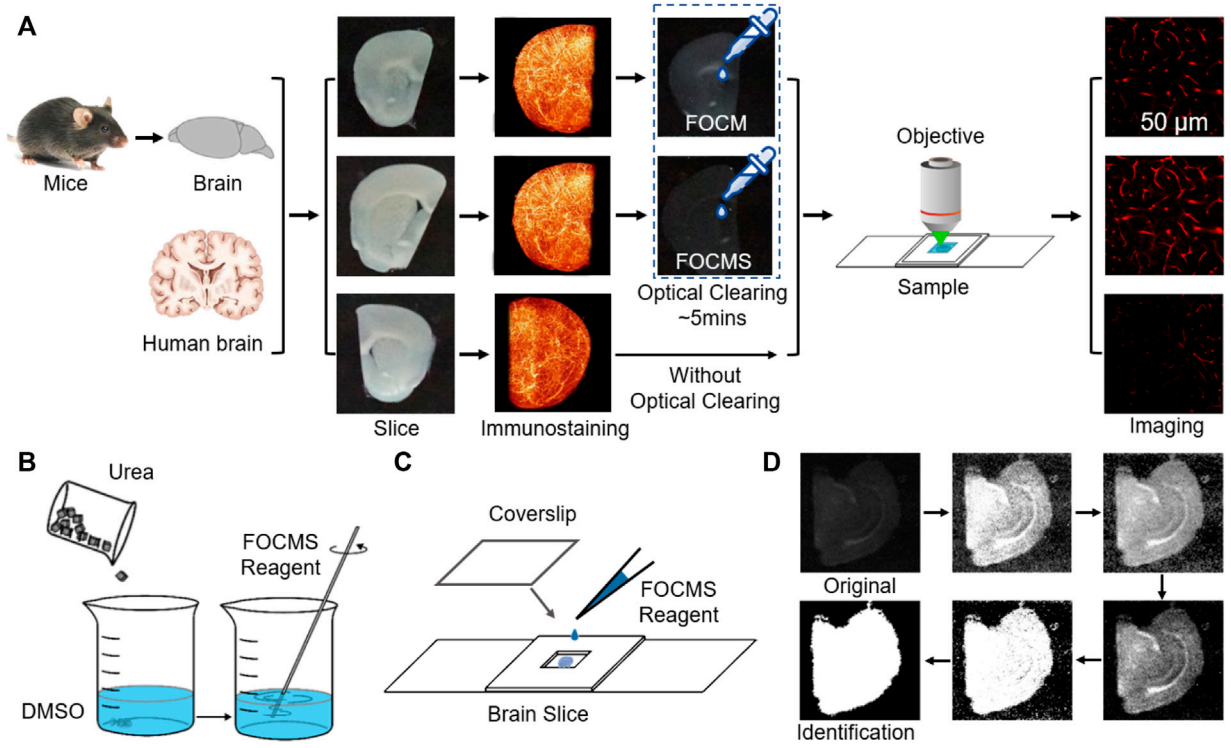

FIGURE 1
FOCMS used for immunostaining imaging and tissue recognition. **(A)** Optical imaging process including brain preparation, slicing, immunostaining, optical clearing and imaging. **(B)** Reagents preparation of FOCM. **(C)** Biological sample clearing and mounting procedure before optical imaging. **(D)** Brain slice range recognition process. The six images are results of normalized, enhancement, pre-recognition, differentiated processing and denoising, binarization of customized threshold and removing isolated noise, respectively. White: brain area, black: background. The sum of white pixels is the area of the brain slice.

UPLSAPO ×60, N.A.1.35, WD 0.15 mm). For maximum intensity projection, the imaging interval on z axis was set as the half of z-axis resolution of different objectives (1.09 μm per slice for ×20 objective, and 0.48 μm per slice for ×60 objective).

Three-Dimensional Reconstruction. The reconstruction method is to find an extremum after preprocessing of normalization, denoising, removing isolated noise, and then use this extremum as the center to judge whether the 26 adjacent points satisfy the requirements of the threshold condition. If the point satisfies the threshold condition, we judged it as cell tissue. The coordinates of cell tissues are considered as the new center, and the fluorescence intensity at the center is used as the new baseline of the threshold. Then it is judged whether the intensity of the surrounding points of the new center satisfies the new threshold condition. Repeat this until no extremum meets the threshold limit and then rejudge whether the reconstructed structure is a cell. Set the reconstructed structure as zero and loop the above process with the next extreme point until there is no extreme point that meets the preset condition.

Transparency Quantitative Analysis Method (TQAM). Transparency was measured by placing the sample in a Petri dish with a black background. The optical clearing process was imaged using a camera (Sony ilce-6000) with the same parameters. The white light source was used to provide uniform brightness and the distance between the sample and the camera was set as 4 cm.

TQAM was achieved using MATLAB R2020a. The detailed procedures are: first, normalize and automatically identify the brightness of the captured images with the assistance of black borders and white grids, and find the black area where the brain slice is located for cropping. Second, enhance the image contrast. Third, binarization and isolated noise are performed to obtain the first pre-identified brain slice area. The threshold of the black area is generally set at a large value to remove noise, while the threshold of the white area sets a small value to prevent the ventricle from being mistaken for an area with brain tissue. However, the coordinates of the brain slice region pre-identified for the first time are often inaccurate because there is no significant difference in average light intensity between the brain slice and outside of the brain slices. To address this,

differentiate the original image to reduce the noise intensity of the background using coordinates of a pre-identified brain slice. Finally, binarize, and remove the isolated noise to obtain the region where the brain slice is located, as shown in Figure 1D.

The means of brightness of the brain area before and after optical clearing are I_{t0} and I_t, respectively. And the average values of the area outside the brain slice before and after optical clearing are I_{b0} and I_b, so the transparency is defined as:

$$\mathbf{T} = \mathbf{1} - \frac{|\boldsymbol{I_t} - \boldsymbol{I_b}|}{|\boldsymbol{I_{t0}} - \boldsymbol{I_{b0}}|}. \quad (1)$$

When T = 0 without optical cleaning, the closer T is to 1, the better the optical cleaning effect. It is worth mentioning that the method is also suitable for the transparency evaluation of other biological tissues and optical clearing methods with proper parameter adjustment. For colored tissues, the brain slice needs to be placed on a Petri dish with a white background, and then the optical clearing process is photographed using a camera. Finally, the tissue area identification and transmittance calculation are performed based on the images.

Sample preparation

Mice and Mouse Brain Samples. Adult mice C57BL/6 and Thy-GFP-M mice were used in the optical clearing and imaging process. Mice were rapidly anesthetized with chloral hydrate (5% wt/vol, 0.1 ml/10 g, intraperitoneal (i.p.)), then transcardially perfused with ice-cold 0.01M PBS (Solarbio) and paraformaldehyde (4% in PBS wt/vol, Sinopharm Chemical Reagent Co., Ltd.). Brain tissues were incubated in the same paraformaldehyde solution at 4°C for 24–48 h for uniform fixation. After fixation, 300-μm-thick brain slices were sectioned using a vibrating slicer (VT 1200S, Leica).

Human Brain Sample. Human brain tissues were fixed in paraformaldehyde at 4°C for 24 h and then 300 μm thick brain slices were sectioned using a vibrating slicer. Before the immunofluorescence staining and optical clearing, the brain slices were incubated in CHAPS and N-Methyldiethanolamine solutions at 4°C for 24 h to remove the influence of the blood.

Antibodies Selection. Primary antibodies: chicken polyclonal anti-GFAP antibody (Abeam, ab4674, dilution 1: 250) for labeling astrocytes; goat polyclonal anti-CD31 antibody (R&D system, AF3628, dilution 1:100) for labeling human vascular endothelial cells; mouse polyclonal anti-CD31 antibody (R&D system, BBA7, dilution 1:100) for labeling vascular endothelial cells.

Secondary antibodies: donkey anti-chicken IgY H&L (FITC) (abcam, ab63507); goat anti-chicken IgY H&L (Alexa Fluor® 647) (abcam, ab150175); donkey anti-goat IgG H&L (Alexa Fluor® 555) (abcam, ab150134); donkey anti-mouse IgG H&L (Alexa Fluor® 647) (abcam, ab150107).

Optical Clearing Reagents Preparing. FOCMS reagent was prepared only using 30% (wt/vol) urea dissolved in DMSO, shown in Figure 1B. FOCM reagent was prepared as 30% wt/vol urea, 20% wt/vol Dsorbitol, and 5% wt/vol glycerol dissolved in DMSO. When preparing the reagent, urea and Dsorbitol were dissolved in DMSO and stirred at room temperature (25°C) overnight. After complete dissolution, glycerol was added and stirred further. The reagents can be stored at room temperature for several months and shaken gently before use.

Results

Optimization of FOCMS using concentration gradient screening

The TQAM method accurately calculates the optical clearing capacity and the area change of the brain tissue, so this method is used for high throughput gradient screening of the optical clearing reagents. Through concentration gradient screening of three solvents (urea, sorbitol and glycerol) used in FOCM for optical clearing, it is found that the optical clearing ability becomes better for the 300 μm brain slice with the decrease of sorbitol concentration (Figure 2A), when the concentration of urea and glycerol are 30% and 5% wt/vol, respectively. At the sorbitol concertation of 20% wt/vol, the transparency of brain slices is only 0.56 within 5 min, while it reaches 0.79 when the sorbitol concertation drops to 0% wt/vol, shown in Figure 2B. The transparency using FOCM achieves 0.76 after 30 min optical clearing, while that of using FOCM reagent with 0% wt/vol sorbitol is up to 0.87 under the same condition. Besides, the FOCM reagent causes severe shrinkage of the brain slice which is less than 60% of the original area and cannot recover to the original size, as shown in Figure 2C. In comparison, the FOCM reagent with 0% wt/vol sorbitol shrinks the brain slice morphology and then swells back to its original size, indicating better tissue morphology preserving ability than that of FOCM. Therefore, the sorbitol in the FOCM reagent reduces the optical clearing effect and causes morphology deterioration. Besides, we found that the increase of glycerol concentration has less influence on optical clearing ability, and deteriorates the brain slice morphology at the urea concentration of 30% wt/vol and the sorbitol concentrations of both 0% and 20% wt/vol.

Compared to FOCM, FOCMS (without sorbitol and glycerol) has the advantages of simpler operation, faster transparency time, better optical clearing effect and less tissue deformation (Figure 2D), especially in areas with higher fiber content and tighter tissues. Using the same concentration gradient screening technology, we analyzed the urea concentration in FOCMS and found that the transparency of the brain slice reaches 0.65 when the urea concentration is 0% (only DMSO solvent). The transparency ability improves with the increase of urea

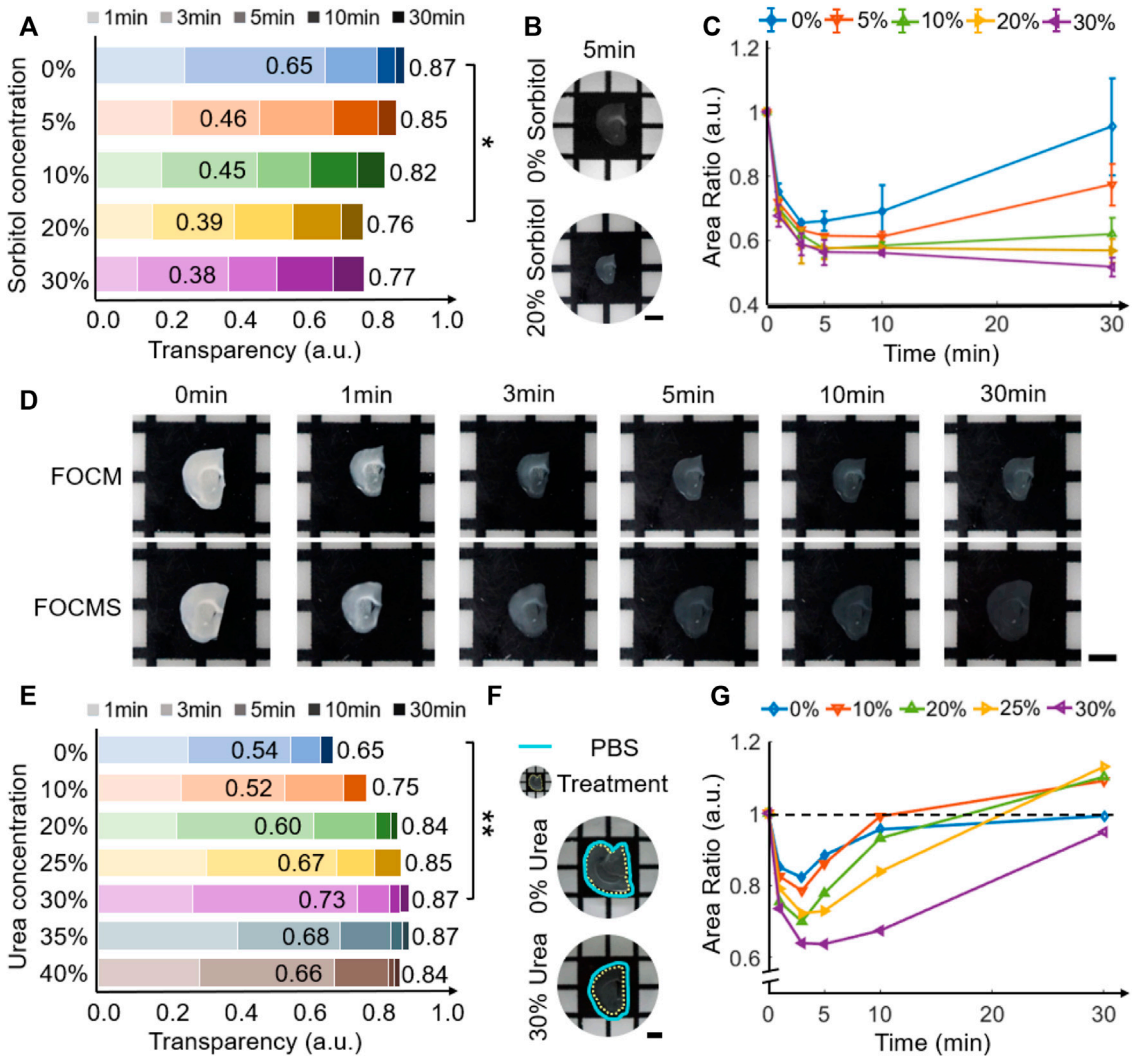

FIGURE 2
FOCM and FOCMS concentration gradient screening. **(A)** Variation of transparency with different sorbitol concentrations in FOCM reagent. **(B)** Comparison of transparency of brain slices using FOCM reagent with sorbitol concentration of 0% and 20% wt/vol for 5 min. **(C)** Changes of brain tissue area with sorbitol concentration in FOCM reagent. **(D)** Comparison of optical clearing effects between FOCM and FOCMS at 0 min, 1 min, 3 min, 5 min, 10 min and 30 min **(E)** Variation of transparency with different urea concentrations in FOCMS reagent. **(F)** Morphology caused by FOCMS reagents. The cyan solid line is the slice boundary before optical clearing, and the yellow dotted line is after optical clearing. **(G)** Changes of brain tissue area with urea concentration in FOCMS reagent. Scaler bar: 2 mm, statistical significance (**$p < 0.01$, *$p < 0.05$).

concertation from 0% to 30% wt/vol, shown in Figure 2E. At the urea concentration of 30% wt/vol, the transparency of brain slice using FOCMS is 0.73 at 3 min, then increase to more than 0.8 at 5 min and finally reaches up to 0.87, while that of using FOCM is up to 0.76 at the same condition. When the urea concentration continues to rise, the optical clearing effect deteriorates. Thus, FOCMS has the best optical clearing ability when the urea concentration is 30% wt/vol. During the optical clearing using FOCMS, brain slices shrink rapidly within 30 min first, and reach the most at 3 min, but gradually recover. Moreover, the morphology of brain slices has severe changes with the rise of the urea concentration increase. When the urea concentration is 30% wt/vol, the area shrinks the most at 3 min, reaching about 64% of the original area, and then gradually recovers, shown in Figure 2F,G. When the urea concentration exceeds 30% wt/vol, the changes in brain area are similar to that of 30% wt/vol. The area difference between and after optical clearing is less than 15% and there are minor changes after 30 min of the optical clearing. Therefore, optical clearing has an optimal time of about 5 min.

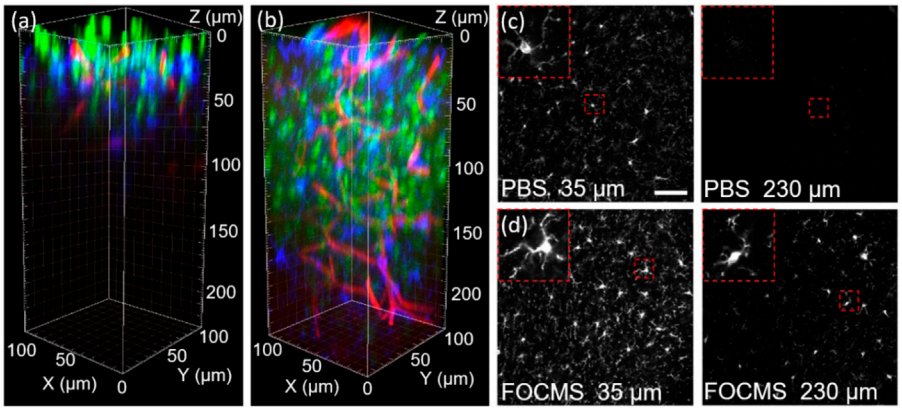

FIGURE 3
Fluorescence imaging of brain tissue **(A)** before and **(B)** after optical clearing. Green: nucleus, blue: glia cell, red: blood vessel. Comparison of glia cell imaging at the depth of 35 μm and 230 μm **(C)** before and **(D)** after clearing, respectively. Scalebar: 50 μm.

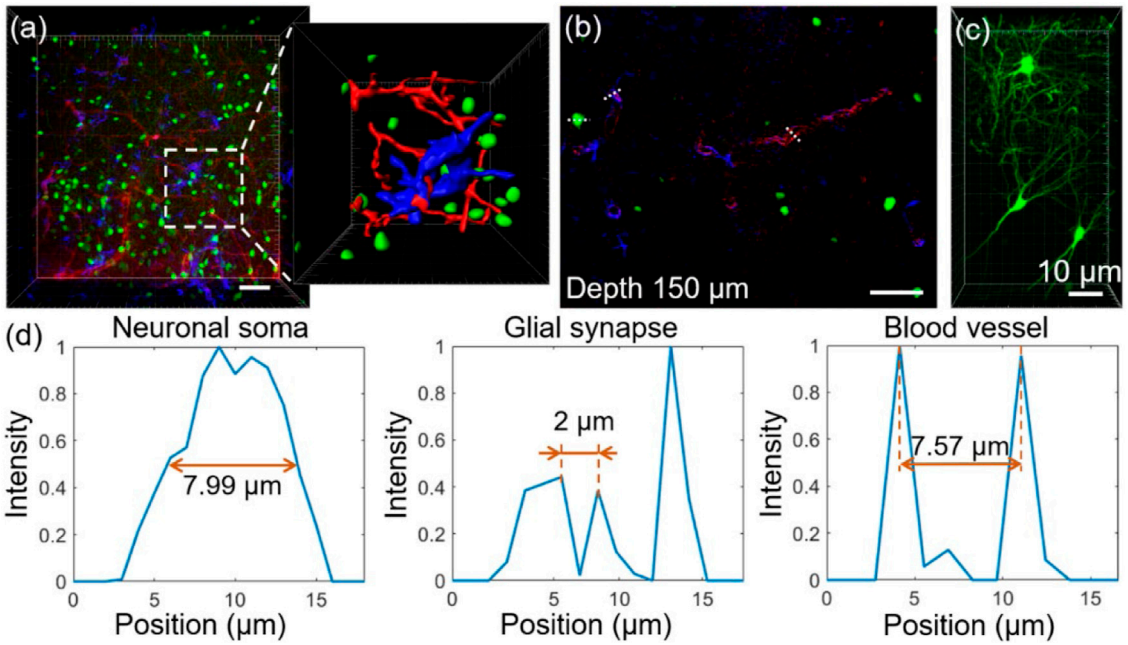

FIGURE 4
Fluorescence imaging quality after FOCMS. **(A)** Imaging of brain tissue with detailed structure exhibition after FOCMS clearing. Green: neurons, blue: glia cell, red: blood vessel. **(B)** Selected single imaging at the depth of 150 μm in **(A)**. **(C)** Imaging of neurons with high NA objective lens. Scale bar: 10 μm **(D)** Normalized fluorescence corresponding to the neuronal Soma, glial synapse, and blood vessel at the depth of 150 μm in **(B)** indicated by the dashed line, respectively. Scale bar: 50 μm.

Imaging depth and quality improvement using FOCMS

FOCMS achieves rapid optical clearing for biological tissues with simple operation, which greatly benefits the improvement of the imaging depth and resolution of fluorescence microscopy. Figure 3 compares the imaging of brain tissues before and after optical clearing using LSCM. Without optical clearing, the range of clear imaging is only about 50 μm. The SNR ratio is greatly reduced after the imaging depth of 50 μm. The SNR ratio drops

with the increase of imaging depth. At the depth of 100 μm, no more effective information is obtained when the SNR ratio is close to 0 (Figure 3A). However, the imaging depth improves to 230 μm using FOCMS, and the SNR maintains almost unchanged, shown in Figure 3B. Figures 3C,D are the imaging of glia cells at the depth of 35 and 230 μm before and after FOCMS clearing, and the upper left corner is an enlarged view of a single glia cell.

Comparing the results of Figures 3C,D, it can be seen that the synaptic intensity of glia cells after optical clearing is significantly stronger than that of before clearing, the number of glia cells is greater and the morphology preserves better, indicating that optical clearing using FOCMS significantly improves the imaging quality even in the imaging depth of LSCM (50 μm). When the depth reaches 230 μm, there is almost no effective information remaining before optical clearing, while after light clearing, some of the glial cells are still resolved, and the synapses are clearly visible.

We further evaluated the results of deep tissue imaging using the FOCMS clearing technique. Figure 4A shows the LSCM imaging after FOCMS clearing, in which neurons are in green, glial cells in blue, and blood vessels in red. The sub-image on the right is the enlarged part of the white dashed box in Figure 4A to show the detailed three-dimensional morphological structures of neurons, glial cells and blood vessels. It is clearly seen that the synapses of glial cells and the vascular walls of blood vessels in Figure 4B show the selected single imaging at the depth of 150 μm in (a). LSCM imaging with high NA clearly displays the dendrites and axons of neurons (Thy1-GFP-M mice) with an imaging resolution higher than 1 μm, as shown in Figure 4C. Figure 4D shows the normalized fluorescence intensity of neuronal Soma, glial synapse and blood vessel in (b), where the full width at half maximum (FWHM) of neuronal Soma is 7.99 μm, and the minimum distance between the three glial synapses is 2 μm and the diameter of the blood vessel is 7.57 μm, respectively. It can be found that when the imaging depth is 150 μm, the structure of cells and tissues still has a high signal-to-noise ratio. We also found that the structures of cells and brain tissues still have a high signal-to-noise ratio at the imaging depth of 150 μm. Therefore, the FOCMS optical clearing technology on brain tissues shows significant improvements in the imaging depth of the microscopic imaging system. Besides, the FOCMS does not quench the exogenous fluorescence like immunofluorescence and chemical dyes and the endogenous fluorescence such as GFP, indicating its excellent fluorescence retention ability.

Applications in human brain tissue with FOCMS

FOCMS significantly improves the depth and quality of imaging with minimal time and effort which shows great potential in the applications of clinical diagnosis and treatment, pathological analysis, *etc.* Here, we demonstrated an application using FOCMS in human brain tissue imaging. As shown in Figures 5A,B describe the three-dimensional LSCM imaging of normal human cerebral blood vessels and brain glioma (GBM) without optical clearing, respectively. The top left image is the original imaging result, the top right image is the detailed structure of blood vessel morphology, and the bottom two images are the selected single imaging at the depth of 50 μm (left) and 200 μm (right) in (a) (b), respectively. Unfortunately, using these imaging results without optical clearing, the morphological differences are not sufficient to distinguish between normal human brain tissue and glioma, and pathological analysis cannot be performed.

After using FOCMS, three-dimensional imaging of normal human brain tissue and glioma are shown in Figures 5C,D, respectively. Among them, the top left image is the original result of imaging, the top right is the detailed structure of blood vessel morphology, and the bottom two images are the selected single imaging at the depth of 50 μm (left) and 200 μm (right), respectively. Owning to the FOCMS optical clearing, the morphological differences between normal human brain tissue and glioma are obvious. Compared to normal blood vessels, blood vessels of glioma are lump-shaped, with tortuous, disordered structure, and enlarged diameter. Therefore, FOCMS technology demonstrates the ability that it can be used to solve the problem of unclear boundary identification of glioma.

Unlike mouse brain tissues, human brain tissues have higher fiber content, greater cell density, tighter tissues, and many impurities, which severely reduces the optical clearing effect. Compared to FOCM, we found that FOCMS technology has a better optical clearing effect on human brain tissue and smaller morphological changes, shown in Supplementary. Comparing the results in the white dotted circles in Figures 5A,C, it is found that there is no significant difference in the morphology of human cerebral blood vessels before and after optical clearing. Figure 5E,G shows the three-dimensional morphology of normal human cerebral blood vessels before (yellow) and after (red) FOCMS optical clearing, respectively, and found that they are well merged. Besides, there is no significant difference in the vascular morphology of gliomas before and after FOCMS optical clearing as well, indicating that the FOCMS technology will not cause obvious deviation in the imaging results of brain tissues.

Since there is no ideal imaging for comparison in practical applications, we use a three-dimensional reconstruction algorithm to separate the signal from the noise for the calculation of the signal-to-noise ratio (SNR). SNR is defined as:

$$\mathbf{SNR} = \mathbf{10} \times \mathbf{log}_{\mathbf{10}}\frac{\boldsymbol{I_s}}{\boldsymbol{I_n}}, \tag{2}$$

10.3389/fphy.2022.1037821

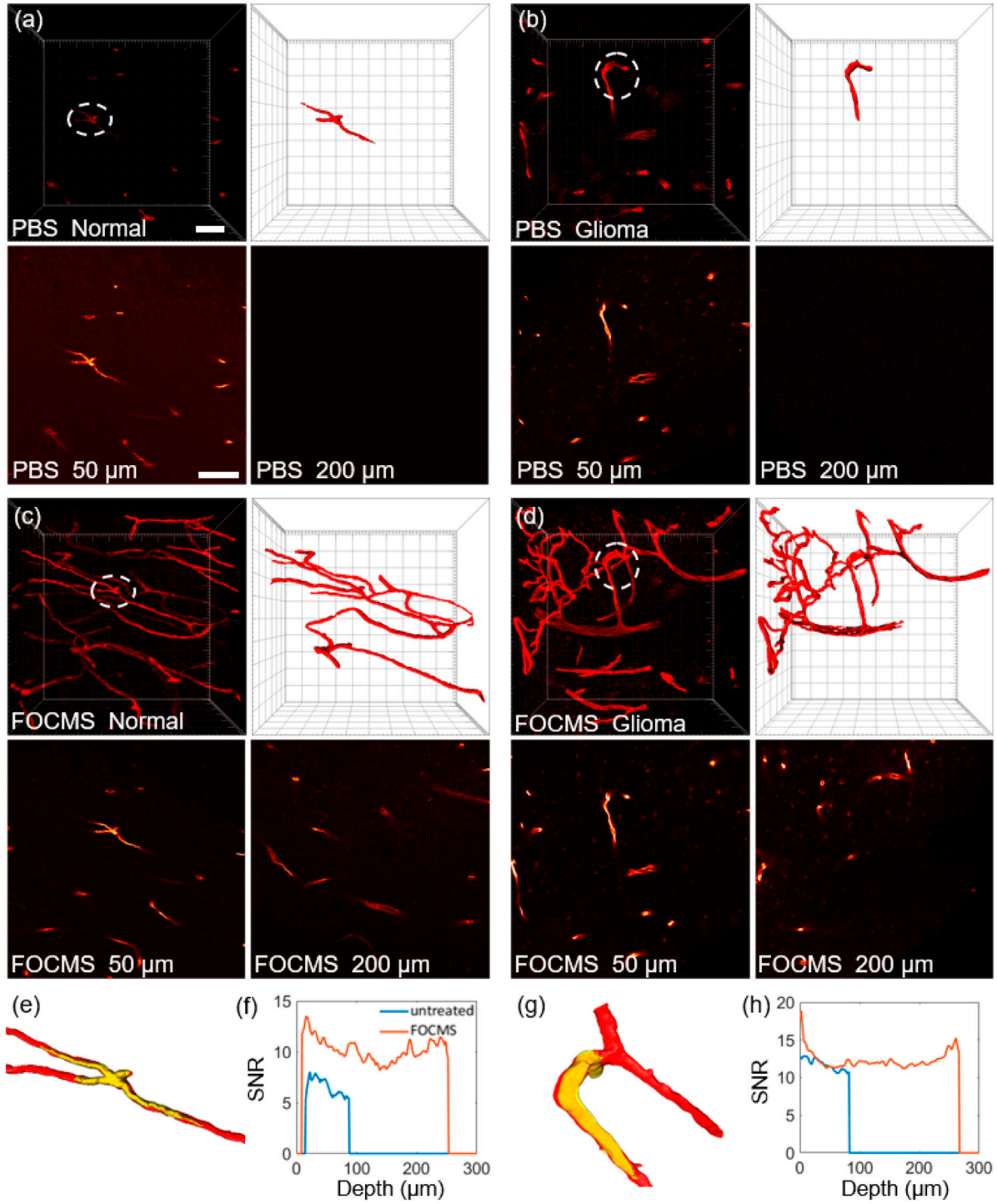

FIGURE 5
Application of FOCMS in human brain tissue imaging. Comparison of three-dimensional imaging of **(A)** normal human brain tissue and **(B)** glioma without optical clearing. Top left: the original imaging, top right: detailed structure of blood vessel morphology, bottom: selected single imaging at the depth of 50 μm (left) and 200 μm (right) in **(A)** and **(B)**, respectively. After using FOCMS, three-dimensional imaging of **(C)** normal human brain tissue and **(D)** glioma, respectively. Top left: the original imaging, top right: detailed structure of blood vessel morphology, bottom: selected single imaging at the depth of 50 μm (left) and 200 μm (right) in **(C)** and **(D)**, respectively. Comparison of **(E)** morphology changes and **(F)** SNR of normal brain tissue before and after FOCMS. **(G)** Morphology changes and **(H)** SNR for glioma with and without optical clearing. Scale bar: 50 μm.

where I_s the mean of signal and I_n is the mean of noise. The final SNR of multiple immunofluorescence staining is the mean of each channel.

Figures 5F,H represent the SNR of 3D imaging at different imaging depths with normal human brain tissue and glioma, respectively. The blue line represents before optical clearing and the orange line represents after optical clearing. For both normal human brain tissue and glioma, the results show that the SNR after optical clearing is higher than that of before optical clearing at the imaging depth of 50 μm (the range of LSCM) and 200 μm. The mean SNR of normal human brain tissue before optical clearing is 6.54, while it reaches 10.23 after FOCMS clearing. For glioma tissue, the mean SNRs are 11.72 and 12.33 before and after optical clearing, respectively. The SNR of glioma tissue is higher than that of normal human brain tissue, which may be due to the changes in the composition of brain tissue during carcinogenesis. With the increase of imaging depth, the SNR without optical clearing gradually decreases. However, the SNR after FOCMS clearing decreases first and then increases, mainly due to the staining effect of the middle position of the tissue during the staining process being worse than that of the edge position. In summary, the FOCMS method effective improve the imaging depth and quality of human brain tissues without changing the tissue morphology, demonstrating the applications in clinical diagnosis and treatment and pathological analysis.

Conclusion

In this paper, we propose a new technology, FOCMS, using a new reagent consisting of only DMSO and urea for optical clearing with better performance. The results show that the transparency reaches 0.73 which is an 87.2% improvement compared to that of FOCM when the urea concentration is 30% wt/vol at the optical clearing time of 3 min. It is achieved owing to the TQAM we proposed based on the brain slice area recognition technique. This method accurately calculates the transparency of optical clearing reagents and the morphological changes in brain slices. Furthermore, high-throughput gradient screening is performed on the reagent composition, concentration, processing time and other parameters of the optical clearing technology using this method. Using the TQAM, we analyze the influences on the three solutes (urea, sorbitol and glycerol) of FOCM *via* concentration gradient screening. It is found that the increased sorbitol concentration reduces the optical clearing effect and prevents morphological shrinkage from returning to the pre-clearing area. Moreover, glycerol has less effect on optical clearing and made the area change more severe. Compared to FOCM, FOCMS without sorbitol and glycerol reagents has the advantages of simpler operation, faster transparency, better optical clearing effect, and less morphological change.

The FOCMS technology achieves ultra-fast and effective optical clearing with little fluorescence quenching only by simply incubating the brain tissue sample for about 5 min. After FOCMS clearing, the results show that the glial cells show stronger synaptic signals, better morphology, and significantly improved imaging quality at the imaging depth of 50 μm. Besides, more than 200 μm of imaging depth is achieved, and the SNR keeps almost unchangeable, enabling clear imaging of neurons and glial synapses, blood vessel walls and other tissues with a resolution of more than 1 μm. Moreover, FOCMS technology does not quench most of the exogenous and endogenous fluorescence and has outstanding fluorescence retention ability. The FOCMS technology has been successfully applied to the human brain tissue and it is shown that FOCMS is superior to FOCM in improvements of optical clearing effect, SNR (56.4% stronger) and preservation of morphology. We also demonstrate an application of solving the problem of unclear identification of brain glioma boundaries, which shows great potential in clinical diagnosis and treatment, pathological analysis, etc.

Data availability statement

The original contributions presented in the study are included in the article/Supplementary Material, further inquiries can be directed to the corresponding author.

Ethics statement

All animal studies were approved by Animal Advisory Committee at Zhejiang University. All of the human specimens were obtained from the Department of Neurosurgery, Second Affiliated Hospital of Zhejiang University School of Medicine. And these studies on human specimens were approved by the Human Research Ethics Committee of the Second Affiliated Hospital of Zhejiang University School of Medicine.

Author contributions

KS, SD, and JZ conceived the concept and designed the study. XXu and JL performed the image processing. YZ, XXi, ZW, and YW performed the experiments. XXu and YZ analyzed the data. All the authors contributed to the preparation of the manuscript.

Funding

National Natural Science Foundation of China (61735016). Key R&D Program of Zhejiang Province (2021C03001). Natural Science Foundation of Zhejiang Province of China (LR22F050007). CAMS Innovation Fund for Medical Sciences (2019-I2M-5-057).

Fundamental Research Funds for the Central Universities. China Postdoctoral Science Foundation (2021M692816).

Conflict of interest

The authors declare that the research was conducted in the absence of any commercial or financial relationships that could be construed as a potential conflict of interest.

Publisher's note

All claims expressed in this article are solely those of the authors and do not necessarily represent those of their affiliated organizations, or those of the publisher, the editors and the reviewers. Any product that may be evaluated in this article, or claim that may be made by its manufacturer, is not guaranteed or endorsed by the publisher.

References

1. Brenna C., Simioni C., Varano G., Conti I., Costanzi E., Melloni M., Neri L. M. Optical tissue clearing associated with 3D imaging: Application in preclinical and clinical studies. *Histochem Cel Biol* (2022) 157, 497PMC9114043–511. doi:10.1007/s00418-022-02081-5

2. Hu Y., Tang W., Cheng P., Zhou Q., Tian X., Wei X., et al. Monitoring circulating tumor cells *in vivo* by a confocal microscopy system. *Cytometry A* (2019) 95(6):657–63. doi:10.1002/cyto.a.23702

3. Wang S., Li Y., Zhao Y., Lin F., Qu J., Liu L. Investigating tunneling nanotubes in ovarian cancer based on two-photon excitation FLIM-FRET. *Biomed Opt Express* (2021) 12(4):1962–73. doi:10.1364/BOE.418778

4. Liu Z., Su W., Ao J., Wang M., Jiang Q., He J., et al. Instant diagnosis of gastroscopic biopsy via deep-learned single-shot femtosecond stimulated Raman histology. *Nat Commun* (2022) 13, 4050PMC9279377. doi:10.1038/s41467-022-31339-8

5. Vu T., Razansky D., Yao J. Listening to tissues with new light: Recent technological advances in photoacoustic imaging. *J Opt* (2019) 21. doi:10.1088/2040-8986/ab3b1a

6. Xu X, Chen J, Zhang B, Huang L, Zheng Y, Si K, et al. Enlarged field of view based on Schwartz modulation for light sheet fluorescence microscopy in deep tissue. *Opt Lett* (2020) 45(17):4851–4. doi:10.1364/OL.398985

7. Zhao S, Todorov MI, Cai R, -Maskari RA, Steinke H, Kemter E, et al. Cellular and molecular probing of intact human organs. *Cell* (2020) 180, 796PMC7557154–812. doi:10.1016/j.cell.2020.01.030

8. Zhu J, Yu T, Li Y, Xu J, Qi Y, Yao Y, et al. Macs: Rapid aqueous clearing system for 3D mapping of intact organs. *Adv Sci (Weinh)* (2020) 7, 81903185. doi:10.1002/advs.201903185

9. Pende M, Vadiwala K, Schmidbaur H, Stockinger AW, Murawala P, Saghafi S, et al. A versatile depigmentation, clearing, and labeling method for exploring nervous system diversity. *Sci Adv* (2020) 6, eaba0365. doi:10.1126/sciadv.aba0365

10. Xu F, Shen Y, Ding L, Yang CY, Tan H, Wang H, et al. High-throughput mapping of a whole rhesus monkey brain at micrometer resolution. *Nat Biotechnol* (2021) 39(12):1521–8. doi:10.1038/s41587-021-00986-5

11. Geng J, Zhang X, Prabhu S, Shahoei SH, Nelson ER, Swanson KS, et al. 3D microscopy and deep learning reveal the heterogeneity of crown-like structure microenvironments in intact adipose tissue. *Sci Adv* (2021) 7(8):eabe2480. doi:10.1126/sciadv.abe2480

12. Ku T, Guan W, Evans NB, Sohn CH, Albanese A, Kim JG, et al. Elasticizing tissues for reversible shape transformation and accelerated molecular labeling. *Nat Methods* (2020) 17, 609PMC8056749–613. doi:10.1038/s41592-020-0823-y

13. Nudell V, Wang Y, Pang Z, Lal NK, Huang M, Shaabani N, et al. HYBRiD: Hydrogel-reinforced DISCO for clearing mammalian bodies, *Nat Methods* (2022) 19, 479PMC9337799–485. doi:10.1038/s41592-022-01427-0

14. Hong SM, Jung D, Kiemen A, Gaida MM, Yoshizawa T, Braxton AM, et al. Three-dimensional visualization of cleared human pancreas cancer reveals that sustained epithelial-to-mesenchymal transition is not required for venous invasion. *Mod Pathol* (2020) 33(4):639–47. doi:10.1038/s41379-019-0409-3

15. Davis FM, Lloyd-Lewis B, Harris OB, Kozar S, Winton DJ, Muresan L, Watson CJ. Single-cell lineage tracing in the mammary gland reveals stochastic clonal dispersion of stem/progenitor cell progeny. *Nat Commun* (2016) 7, 13053. doi:10.1038/ncomms13053

16. Kolesová H, Čapek M, Radochová B, Janáček J, Sedmera D. Comparison of different tissue clearing methods and 3D imaging techniques for visualization of GFP-expressing mouse embryos and embryonic hearts. *Histochem Cel Biol* (2016) 146(2):141–52. doi:10.1007/s00418-016-1441-8

17. Susaki EA, Shimizu C, Kuno A, Tainaka K, Li X, Nishi K, et al. Versatile whole-organ/body staining and imaging based on electrolyte-gel properties of biological tissues, *Nat Commun* (2020) 11. doi:10.1038/s41467-020-15906-5

18. Tainaka K, Murakami TC, Susaki EA, Shimizu C, Saito R, Takahashi K, et al. Chemical landscape for tissue clearing based on hydrophilic reagents. *Cell Rep* (2018) 24(8):2196–210.e9. doi:10.1016/j.celrep.2018.07.056

19. Murray E, Cho JH, Goodwin D, Ku T, Swaney J, Kim SY, et al. Simple, scalable proteomic imaging for high-dimensional profiling of intact systems. *Cell* (2015) 163, 1500PMC5275966–14. doi:10.1016/j.cell.2015.11.025

20. Park YG, Sohn CH, Chen R, McCue M, Yun DH, Drummond GT, et al. Protection of tissue physicochemical properties using polyfunctional crosslinkers. *Nat Biotechnol* (2018) 37:73–83. doi:10.1038/nbt.4281

21. Avilov SV. Navigating across multi-dimensional space of tissue clearing parameters. *Methods Appl Fluoresc* (2021) 9(2):022001. doi:10.1088/2050-6120/abe6fb

22. Zhu X, Huang L, Zheng Y, Song Y, Xu Q, Wang J, et al. Ultrafast optical clearing method for three-dimensional imaging with cellular resolution. *Proc Natl Acad Sci U S A* (2019) 116(23):11480–9. doi:10.1073/pnas.1819583116

23. Liu L, Xia X, Xiang F, Gao Y, Li X, Li H, Zheng W. F-CUBIC: A rapid optical clearing method optimized by quantitative evaluation. *Biomed Opt Express* (2021) 13, 237–51. doi:10.1364/BOE.442976